Navigation Function-Based Control of Multiple Wheeled Vehicles

Augie Widyotriatmo, *Student Member, IEEE*, and Keum-Shik Hong, *Senior Member, IEEE*

Abstract—In this paper, a collision-free navigation method for a group of autonomous wheeled vehicles is investigated. The position and orientation information of individual vehicles is transformed to navigation variables, which are the distance left to the goal position, the angle made by the orientation of the vehicle at the goal position and the vehicle-to-target (v-to-t) vector, and the angle made by the heading direction of the vehicle and the v-to-t vector. As a Lyapunov function for deriving a smooth control law that drives all the vehicles from an initial configuration to a goal configuration, a new navigation function that incorporates the squared norm of the navigation variables, the boundaries of collision-free areas, and the angles made by the vehicle heading direction and the vehicle-to-obstacle (v-to-o) vectors is proposed. The asymptotic stability of the closed-loop system is proved. The effectiveness of the developed algorithm is illustrated through three simulations (three vehicles in a free environment, three vehicles in the presence of a static obstacle, and eight vehicles operating along a corridor) and two experiments (static and moving obstacles avoidance). The proposed algorithm has been implemented on a real forklift and the navigation of the forklift from an arbitrary initial configuration to a goal configuration while avoiding collisions has been demonstrated.

Index Terms—Autonomous navigation, collision avoidance, Lyapunov function, multivehicle system, nonholonomic constraint.

I. INTRODUCTION

MULTIVEHICLE systems have received increasing attention in recent years due to their various applications including soccer robots, material-handling vehicles, military operations, security guards, surveillance systems, etc. The problem discussed in this paper is to obtain a feedback control law that allows multiple vehicles to navigate from one configuration (i.e., position and orientation) to another configuration while avoiding collisions during their navigations. The vehicles used in this paper have two fixed wheels in the front and one driving-and-steering wheel in the rear. Such type of vehicle is commonly used in the material handling industry. In this paper, the use of forklifts in an unmanned warehouse is the focus. In a loading/unloading process, the forklift should approach a pallet/load not only from a precise position, but also with an accurate orientation of the fork.

The wheeled vehicle is a nonholonomic system (a system with nonholonomic constraints). According to Brocket's theorem, a nonholonomic system cannot be stabilized to a goal configuration via continuous and time-invariant state-feedback [1] (i.e., either time-varying and/or discontinuous feedback may provide a solution). Therefore, the steering problem of such systems to a goal configuration as they avoid obstacles, even for a single vehicle, is a difficult task. A number of methods to stabilize (i.e., to steer to a goal configuration) nonholonomic systems have been proposed in the literature; some are open-loop controls [2]–[4] and some are closed-loop controls [5]–[7]. However, most papers address only either stabilization or collision avoidance, but not both at the same time.

The recent issues of multiagent systems include the flocking theory, the rendezvous problem in a given workspace, formation control, etc., [8]–[11]. Several studies have also been devoted to multiagent navigation systems with collision avoidance ability [12]–[16]. An autonomous navigation problem is usually decomposed into three parts [17], [18]: path/trajectory planning [19]–[21], path/trajectory following [22]–[24], and precision control to the desired goal configuration [25]–[27]. However, in order for an autonomous vehicle to be accident-preventive, it should be able to deal with a dynamically changing environment. In this sense, we consider a closed-loop solution based on a navigation function that offers fast online motion replanning of multiple vehicles. After collision-free motion trajectories are determined, a robust control algorithm can be implemented [28] to track their designed trajectories as close as they can.

Several methods have been proposed to steer mobile robots to their destination configurations while they avoid collisions. One method that is commonly used for collision-free navigation is the artificial potential method both for a single robot case [29] and for multiple robots case [30] due to its simplicity and well-established mathematical analysis. However, the fundamental limitations of the artificial potential method include the existence of local minima [30] and the lack of a rigorous proof related to the asymptotical stability of the destination configuration [31]. To solve the local minima problem, a navigation function that assures a global minimum needs to be constructed [32], [33]. In [34], the navigation function proposed in [32], [33] is used as a Lyapunov function candidate and the control law is derived in such a way that the asymptotic stability of the destination configuration is achieved. To deal with the nonholonomic constraints, pseudo-obstacles at both sides of a destination point (in the perpendicular direction of the final orientation) are assigned so that motions approaching

from the perpendicular direction of the goal configuration are restricted. Loizou and Kyriakopoulos [35] showed that their kinematics-based control algorithm induces a chattering behavior for multivehicle systems. To suppress chattering behaviors, they implemented a nonsmooth backstepping control method, which was first proposed by Tanner and Kyriakopoulos [36].

In this paper, the kinematics of a vehicle (forklift) with one driving-and-steering wheel in the rear is first reviewed and the configuration variables of the vehicle are reformulated in the form of navigation variables. The navigation variables are the distance from the vehicle frame (a body coordinate system attached to the vehicle) to the target frame (a desired goal configuration of the vehicle), the angle between the x-axis of the target frame and the v-to-t vector, and the angle between the x-axis of the vehicle frame and the v-to-t vector. By transforming the configuration variables to the navigation variables, the global asymptotic stability of the closed-loop system by a smooth feedback control law can be guaranteed [37].

To add the functionality of collision avoidance to a stabilization control law, a closed-loop algorithm based on a modified navigation function is proposed. This modified navigation function is constructed incorporating a metric that will be introduced in the navigation variables domain, a function that represents the boundaries of the collision-free area, and a metric consisting of the angles between the vehicle orientation and the v-to-o vectors (connecting the vehicle center and the obstacle centers). The metric of the angles made by the vehicle orientation and the v-to-o vectors is included to prevent the vehicle from navigating toward the obstacles. By using the proposed navigation function as a Lyapunov function candidate, a control law that steers the vehicles to their individual destinations without collision is derived and the asymptotic stability of the closed loop system is assured. Moreover, the resulting control signals are smooth without any chattering.

The contributions of this paper are as follows. A new navigation function to achieve both global stabilization and collision avoidance of multiple wheeled vehicles is proposed. The asymptotic stability of the closed-loop control law to steer multiple vehicles from their initial configuration to any configuration while avoiding collision is assured. The proposed method provides a smooth control law and the chattering phenomenon of the closed-loop system response has been eliminated. Finally, experimental results of the proposed algorithm on a real forklift with static and moving obstacles are presented.

The paper is organized as follows. Section II discusses the kinematics of a typical vehicle with one driving-and-steering wheel in the rear. Section III introduces a new navigation function for both stabilization and collision avoidance. Section IV investigates a navigation control law for a single vehicle. Section V extends the navigation control law in Section IV to the case of multiple vehicles. Section VI-A illustrates the navigation of three vehicles in a free environment (no static obstacles) and in the presence of a static obstacle and the navigation of eight vehicles moving along a corridor. Section VI-B shows the experimental results of the forklift reaching a target configuration while avoiding static obstacles and two moving persons. The conclusions are given in Section VII.
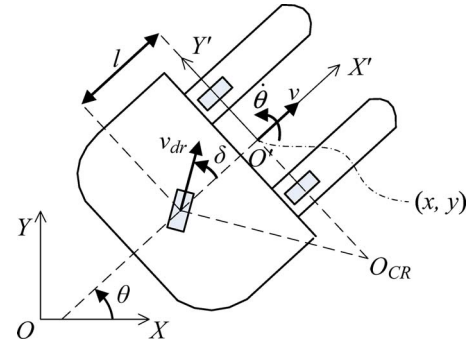
Fig. 1. Forklift with a single driving-and-steering wheel in the rear.

II. VEHICLE MODEL

In this section, we present the kinematics of a wheeled vehicle that has two caster wheels in the front and one driving-and-steering wheel in the rear. In Fig. 1, l represents the distance between the center of the rear wheel and the axis of the front wheels; OXY represents the global coordinate frame that is fixed in the plane of motion; O' denotes the reference point of the vehicle from which the vehicle motions are generated in the global coordinate frame and becomes the origin of the local coordinate frame $O'X'Y'$, which is attached to the vehicle body; and O_{CR} represents the instantaneous center of rotation of the vehicle. A configuration (i.e., position and orientation) of the vehicle is specified by (x, y, θ), where x, y are the coordinates of the reference point O' and θ is the orientation of the local coordinate frame $O'X'Y'$ with respect to the global coordinate frame OXY (in the counter clock-wise direction). The linear and rotational velocities of the vehicle are denoted by v and $\dot{\theta}$, respectively. Two control inputs are the driving velocity v_{dr} and the steering angle δ, both of which are applied at the rear wheel. It is assumed that the rotational motions of all wheels are pure rolling with no slipping.

From Fig. 1, the rotational velocity $\dot{\theta}$ of the vehicle is obtained as follows:

$$\dot{\theta} = -\frac{v_{dr}}{l/\sin\delta} = -\frac{v}{l/\tan\delta}. \tag{1}$$

The negative sign appears in the right-hand side of (1) since the value of $\dot{\theta}$ is negative as the value of δ becomes positive (i.e., the counterclockwise direction). From (1), the relationship among the linear velocity v, the driving velocity v_{dr}, and the steering angle δ is derived as follows:

$$v = v_{dr}\cos\delta. \tag{2}$$

From (1) and (2), the velocities of the reference point O' in the global coordinate frame are obtained as follows:

$$\dot{x} = v_{dr}\cos\theta\cos\delta \tag{3}$$
$$\dot{y} = v_{dr}\sin\theta\cos\delta \tag{4}$$
$$\dot{\theta} = -(v_{dr}/l)\sin\delta. \tag{5}$$

In Fig. 2, let O'' be a given target point in the global coordinate frame, on which the target coordinate frame $O''X''Y''$ is attached. The desired goal configuration is denoted by (x_d, y_d, θ_d), where x_d, y_d are the coordinates of the target point
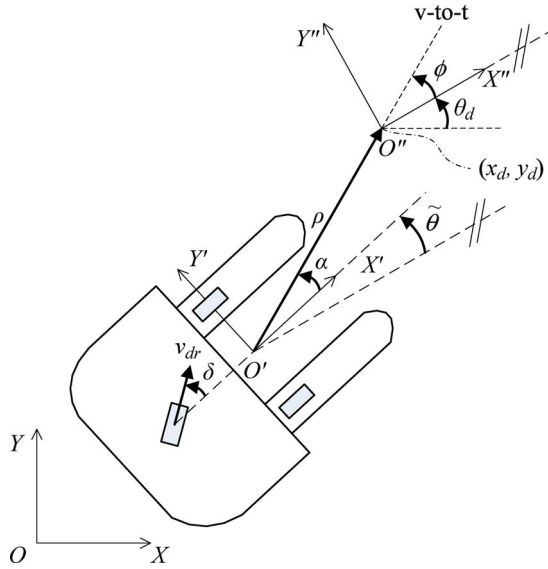
Fig. 2. Coordinates and navigation variables (ρ, ϕ, α).

Fig. 3. Circular-shaped representations of the vehicle and the ith obstacle.

O'' and θ_d is the orientation of $O''X''Y''$ from OXY. The v-to-t vector is defined as a vector connecting O' and O''.

To design a smooth control law that drives the vehicle from an initial configuration to the goal configuration, three navigation variables ρ, ϕ, and α are introduced as follows: ρ is the distance between O' and O'', which is $\rho = \sqrt{(x_d - x)^2 + (y_d - y)^2}$; ϕ is the angle made by the X''-axis of the target coordinate frame $O''X''Y''$ and the v-to-t vector, which is $\phi = \mathrm{atan2}(y_d - y, x_d - x) - \theta_d$; and α is defined as the angle between the X'-axis of the local coordinate frame $O'X'Y'$ and the v-to-t vector, which is $\alpha = \phi - \widetilde{\theta}$, where $\widetilde{\theta} = \theta - \theta_d$. With the introduction of navigation variables from configuration variables, we can say that the origin of the space made by navigation variables becomes $(\rho, \phi, \alpha) = (0, 0, 0)$, which corresponds to the realization of a target configuration in the Cartesian coordinate frame, that is, $(x, y, \theta) = (x_d, y_d, \theta_d)$.

The kinematics equations (3)–(5) can be rewritten using the navigation variables (ρ, ϕ, α) as follows:

$$\dot{\rho} = -v_{dr} \cos \alpha \cos \delta \qquad (6)$$
$$\dot{\phi} = (v_{dr}/\rho) \sin \alpha \cos \delta \qquad (7)$$
$$\dot{\alpha} = (v_{dr}/\rho) \sin \alpha \cos \delta + (v_{dr}/l) \sin \delta \qquad (8)$$

where $\dot{\widetilde{\theta}} = \dot{\theta}$ has been assumed since θ_d is constant. In this paper, it is assumed that the steering angle δ is in the range of $\delta \in (-\pi/2, \pi/2)$. The boundedness of the steering angle is true for most wheeled vehicles, particularly, in the case of forklifts.

III. NAVIGATION FUNCTION

The navigation function is a function in which the negative gradient of the function induces the vehicle to be attracted toward a desired configuration and repelled against obstacles [33]. The main idea behind the navigation function method is to design a control law, which is formed by the negated gradient of the navigation function, so that the system is driven from an initial configuration to a goal configuration as the elements in the system avoid collisions.

In Fig. 3, both the vehicle and the ith obstacle are represented as circular objects. Let r and r_i be the radii of the vehicle and the ith obstacle, respectively. For collision avoidance with the ith obstacle, a new variable γ_i (as a quadratic function of the position values (x, y) of the vehicle accounting for the radii (sizes) of the vehicle and the ith obstacle) is introduced as follows:

$$\gamma_i(x, y) = \rho_i^2(x, y; x_i, y_i) - (r + r_i)^2$$
$$= (y - x_i)^2 + (y - y_i)^2 - (r + r_i)^2 \qquad (9)$$

where $\rho_i = \sqrt{(x - x_i)^2 + (y - y_i)^2}$ is the distance from the vehicle to the ith obstacle and (x_i, y_i) denotes the center of the ith obstacle. Then, the collision area of the vehicle to the ith obstacle, E_i, is defined as follows:

$$E_i = \{(x, y) \in W : \quad \gamma_i(x, y) < 0\} \qquad (10)$$

where W denotes the total workspace of the vehicle with zero obstacle. Let $\cup_{i=1}^n E_i$, $i = 1, 2, \ldots, n$, be the union of all possible collision areas to n obstacles. The collision-free space F is found by removing all the collision areas from W, that is, $F = W - \cup_{i=1}^n E_i$. Then, the boundary of the collision-free area of the vehicle for the ith obstacle, K_i, is defined as follows:

$$K_i = \{(x, y) \in F : \quad \gamma_i(x, y) = 0\}. \qquad (11)$$

Finally, a real-valued map $\Gamma : F \to R^+$, which will be used in the navigation function to access collision-free areas, is defined as follows:

$$\Gamma = \prod_{i=1}^n \gamma_i. \qquad (12)$$

As a result, the zero value of Γ becomes the boundary of F.

Definition 1 [32]: Let F be a collision-free area for an autonomous vehicle and let (x_d, y_d) be the goal position in the interior of F. A map $V_h : F \to [0, 1]$ is a navigation function if it is smooth on F (at least a C^2 function), has a unique minimum at (x_d, y_d), is uniformly maximal on the boundary

of F, and is a Morse function (i.e., the initial conditions that will bring the system to saddle points are sets of measure zero).

The following navigation function was introduced in [32]:

$$V_h = \frac{\rho^2}{(\rho^{2\kappa} + \Gamma)^{1/\kappa}} \tag{13}$$

where κ is a tuning parameter so that (13) satisfies Definition 1. However, this navigation function does not consider the nonholonomic constraints of the vehicle. Therefore, we extend the navigation function (13) to systems with nonholonomic constraints.

First, the squared norm of the navigation variables is used as a metric to determine the closeness between the initial configuration and the goal configuration as follows:

$$z = k_\rho \rho^2 + k_\phi \phi^2 + k_\alpha \alpha^2 \tag{14}$$

where k_ρ, k_ϕ, and k_α are positive constants. Instead of using (12) that configures only the collision area, we propose to include a metric associated with the angles between the v-to-o vectors and the vehicle orientation; for the ith obstacle, this angle becomes $\beta_i = \mathrm{atan2}(y_i - y, x_i - x) - \theta$, where $\theta \in \Theta$ is an arbitrary orientation of the vehicle, and the metric includes β_i^2. Therefore, a real-valued map $\mathrm{B} : F \times \Theta \to R^+$ is defined as follows:

$$\mathrm{B} = \prod_{i=1}^n \beta_i^2. \tag{15}$$

Accordingly, the (x, y, θ) set where $\mathrm{B} = 0$ represents the vehicle configurations directed to the obstacles.

The novelty of combining two real-valued maps (12) and (15) in a new navigation function comes from the fact that a vehicle configuration that is close to and is directed to obstacles should be avoided. Finally, a new navigation function for both stabilization and obstacle avoidance is proposed as follows:

$$V_{\mathrm{nh}} = \frac{1}{2} \frac{z}{(z^\kappa + k_\gamma \Gamma + k_\beta \mathrm{B})^{1/\kappa}} \tag{16}$$

where k_γ and k_β are positive constants and the subscript nh stands for nonholonomic. A systematic method to determine the value of κ is provided in the Appendix.

IV. STABILIZATION OF A SINGLE VEHICLE

A. Stabilization

First, we design a control law to steer the vehicle described in Section II from an initial configuration to the goal configuration without considering collision avoidance.

Proposition 1: Consider the system (6)–(8). The origin of the closed-loop system under the control law

$$v_{dr} = k_{v_{dr}} \rho \cos \alpha \tag{17}$$

$$\delta = -\tan^{-1}\left(\frac{l}{k_{v_{dr}} \rho \cos \alpha} \left(k_{\alpha c} \alpha + (k_\alpha \alpha + k_\phi \phi) \right. \right.$$
$$\left. \left. \times \frac{k_{v_{dr}} \cos \alpha \sin \alpha}{k_\alpha \alpha} \right) \right) \tag{18}$$

where $k_{v_{dr}}$ and $k_{\alpha c}$ are positive constants, is asymptotically stable.

Proof: Let the squared norm of the navigation variables in (14) serve as a Lyapunov function V. The derivative of the chosen Lyapunov function can be written as

$$\dot{V} = 2(k_\rho \rho \dot{\rho} + k_\phi \phi \dot{\phi} + k_\alpha \alpha \dot{\alpha}). \tag{19}$$

The substitution of (6)–(8) and (17) and (18) into (19) yields

$$\dot{V} = -2\left(k_{v_{dr}} k_\rho \rho^2 \cos^2 \alpha + k_{\alpha c} k_\alpha \alpha^2 \right) \cos \delta \le 0 \tag{20}$$

where $\delta \in (-\pi/2, \pi/2)$, which implies the negative semidefiniteness of the Lyapunov function. From (20), we can conclude that the Lyapunov function V is always nonincreasing in time and asymptotically converging to a non-negative value. In turn, the state trajectory from any initial condition is always bounded. From (20), ρ and α are square integrable and are uniformly continuous due to the existence of their derivatives. Therefore, by Barbalat's lemma, ρ and α converge to zero.

Now, we show that the value of ϕ also converges to zero. By applying (17) and (18) to (6)–(8), the closed-loop system becomes

$$\dot{\rho} = -k_{v_{dr}} \rho \cos^2 \alpha \cos \delta \tag{21}$$

$$\dot{\phi} = k_{v_{dr}} \cos \alpha \sin \alpha \cos \delta \tag{22}$$

$$\dot{\alpha} = \left(-k_{\alpha c} \alpha - k_{v_{dr}} k_\phi \phi \cos \alpha \sin \alpha / (k_\alpha \alpha) \right) \cos \delta. \tag{23}$$

From (21) and (22), we can conclude that both $\dot{\rho}$ and $\dot{\phi}$ converge to zero since ρ and α converge to zero. This implies that ϕ approaches a finite limit $\bar{\phi}$ as time increases. From (23), it can be seen that the value of $\dot{\alpha}$ approaches $-(k_{v_{dr}} k_\phi / k_\alpha) \bar{\phi} \cos \delta$. Since α converges to zero and $\dot{\alpha}$ is a uniformly continuous function, based on Barbalat's lemma, $\dot{\alpha}$ must converge to zero. Therefore, the value of the finite limit $\bar{\phi}$ must be necessarily zero. This proves the asymptotic stability of the origin of the closed-loop system. ∎

By using (18), it can be seen that the derivative of the Lyapunov function (20) is less than zero, thus α goes to zero. However, α might be unbounded when the measurement noises and the input disturbances are present, particularly when α is a small value. To solve this problem, a switching control method is recommended to handle the measurement noises and to reject the input disturbances of the system, as suggested in [38]–[40].

From the closed-loop system (21)–(23), the rates of convergence of the variables ρ, ϕ, and α to the origin are tuned by adjusting the parameters $k_{v_{dr}}$, $k_{\alpha c}$, k_ϕ, and k_α. It is noted that the stabilization of the closed-loop system is independent of the parameter k_ρ, but it will play a role in the collision avoidance below.

B. Stabilization With Collision Avoidance

In this section, we derive a control law for stabilization with collision avoidance by using the proposed navigation function (16) as a Lyapunov candidate. To design the stabilization

control law with collision avoidance, new variables are introduced as follows:

$$\overline{\rho} = \psi'_\gamma(z/\kappa) \sum_{i=1}^n (\rho_i/\gamma_i) \cos \beta_i \tag{24}$$

$$\overline{\alpha} = \psi'_\beta \left(z/(\kappa k_\alpha \alpha) \right) \sum_{i=1}^n \left(1/|\beta_i| \right) \tag{25}$$

$$\overline{\xi} = \psi'_\beta \frac{z}{\kappa k_\alpha \alpha} k_{v_{dr}} (k_\rho \rho \cos \alpha - \overline{\rho}) \sum_{i=1}^n \frac{\sin \beta_i}{|\beta_i| \rho_i} \tag{26}$$

where

$$\kappa \neq \psi'_\gamma z / (k_\rho \rho \cos \alpha) \sum_{i=1}^n (\rho_i/\gamma_i) \cos \beta_i \tag{27}$$

$$\psi'_\gamma = \psi_\gamma / (\psi_\gamma + \psi_\beta) \tag{28}$$
$$\psi'_\beta = \psi_\beta / \psi_\gamma + \psi_\beta \tag{29}$$

$$\psi_\gamma = \left(k_\gamma \prod_{i=1}^n \gamma_i \right) \Big/ \left(z^\kappa + k_\gamma \prod_{i=1}^n \gamma_i + k_\beta \prod_{i=1}^n \beta_i^2 \right)^{\frac{1}{\kappa}+1} \tag{30}$$

$$\psi_\beta = \left(k_\beta \prod_{i=1}^n \beta_i^2 \right) \Big/ \left(z^\kappa + k_\gamma \prod_{i=1}^n \gamma_i + k_\beta \prod_{i=1}^n \beta_i^2 \right)^{\frac{1}{\kappa}+1}. \tag{31}$$

The dynamics of obstacle variables γ_i and β_i can be described by the following equations:

$$\dot{\gamma}_i = -2\rho_i v_{dr} \cos \beta_i \cos \delta \tag{32}$$
$$\dot{\beta}_i = (v_{dr}/\rho_i) \sin \beta_i \cos \delta + (v_{dr}/l) \sin \delta. \tag{33}$$

We now state the following kinematic control law.

Proposition 2: Consider the system (6)–(8). The origin $(\rho, \phi, \alpha) = (0, 0, 0)$ of the closed-loop system under the control law

$$v_{dr} = k_{v_{dr}} (k_\rho \rho \cos \alpha - \overline{\rho}) \tag{34}$$

$$\delta = -\tan^{-1} \Bigg(\frac{l}{k_{v_{dr}} (k_\rho \rho \cos \alpha - \overline{\rho})} $$
$$\times \left(k_{\alpha c} \alpha (1 - \overline{\alpha}) + \frac{k_{v_{dr}} (k_\alpha \alpha + k_\phi \phi)}{k_\alpha \alpha} \right. $$
$$\left. \times \left(k_\rho \cos \alpha - \frac{\overline{\rho}}{\rho} \right) \sin \alpha - \overline{\xi} \right) \Bigg) \tag{35}$$

is asymptotically stable.

Proof: Let the navigation function in (16) be a Lyapunov function candidate. The time derivative of the Lyapunov function is examined as follows:

$$\dot{V}_{\text{nh}} = \frac{\partial V_{\text{nh}}}{\partial \rho} \dot{\rho} + \sum_{i=1}^n \frac{\partial V_{\text{nh}}}{\partial \gamma_i} \dot{\gamma}_i + \frac{\partial V_{\text{nh}}}{\partial \phi} \dot{\phi} $$
$$+ \frac{\partial V_{\text{nh}}}{\partial \alpha} \dot{\alpha} + \sum_{i=1}^n \frac{\partial V_{\text{nh}}}{\partial \beta_i} \dot{\beta}_i. \tag{36}$$

By using (6)–(8), (24)–(26), (32) and (33), and the control law (34) and (35), the time derivative (36) becomes

$$\dot{V}_{\text{nh}} = (\psi_\gamma + \psi_\beta) \Bigg(- k_{v_{dr}} (k_\rho \rho \cos \alpha - \overline{\rho})^2 - k_{\alpha c} k_\alpha \alpha^2 (1 - \overline{\alpha})^2 $$
$$+ \overline{\alpha} \left(k_{v_{dr}} (k_\alpha \alpha + k_\phi \phi) \left(k_\rho \cos \alpha - \frac{\overline{\rho}}{\rho} \right) \sin \alpha - k_\alpha \alpha \overline{\xi} \right) \Bigg) \cos \delta. \tag{37}$$

The positive term in (37) restrains the convergence of the navigation variables to zero. However, when the vehicle is not close to and is not directed to obstacles, the values of $\overline{\rho}$, $\overline{\alpha}$, and $\overline{\xi}$ are small, while at the origin, the value of $\overline{\rho} = \overline{\alpha} = \overline{\xi} = 0$ since $z = 0$. Thus, (37) will be in a semidefinite form as in (20). Accordingly, the control law (34) and (35) drives the navigation variables ρ, ϕ, and α to go to zero as already verified in the proof of Proposition 1.

Now, let $S = \{(\rho, \phi, \alpha) : 0 \in \dot{V}_{\text{nh}}\}$. By inequality (27), the value $v_{dr} = 0$ occurs only at $(\rho, \phi, \alpha) = (0, 0, 0)$. Therefore, the set $S = \{(\rho, \phi, \alpha) : \dot{V}_{\text{nh}} = 0\}$ contains no trajectories of the system, except the trajectory $(\rho, \phi, \alpha) = (0, 0, 0)$ for $t \geq 0$. By applying LaSalle's invariance principle, every trajectory from any initial condition of the closed-loop system converges to zero. ∎

From (34), we can see that the value of $\overline{\rho}$ influences the value of v_{dr}. If the vehicle configuration is far from and is not directed to obstacles, then the value of $\overline{\rho}$ becomes small. In turn, the driving velocity v_{dr} behaves like the control law in (17). Conversely, if the vehicle configuration is close to and is directed to obstacles, then the value of $\overline{\rho}$ becomes large. In this case, the value of v_{dr} decreases.

From (35), the value of $\overline{\alpha}$ and $\overline{\xi}$ influence the value of δ, where δ and v_{dr} determine the direction of the vehicle. If the vehicle configuration is directed to obstacles, then the value of $\overline{\alpha}$ becomes large. From the derivative of the Lyapunov function (37), if the value of $\overline{\alpha}$ is large and the third term of (37) yields a positive value, then the rates of convergence of the navigation variables to zero are restrained. This permits the vehicle to turn away from the direction to the target to avoid collisions.

In (34), k_ρ becomes a gain to the driving velocity; k_γ becomes a gain to the value of ψ_γ and consequently, increases the value of $\overline{\rho}$, where the large value of $\overline{\rho}$ suppresses the driving velocity v_{dr} in the area that is close to and is directed to obstacles. In (35), k_β becomes a gain to the value of ψ_β and accordingly increases the value of $\overline{\alpha}$, which provides a gain to the steering angle δ to drive the vehicle away from the origin of the target coordinate when the vehicle is close to and is directed to obstacles.

V. MULTIPLE VEHICLES SYSTEM

In this section, the navigation control law developed for a single vehicle in Section IV is extended to a multivehicle system. The type of vehicles in the system is assumed to be the same, that is, the typical vehicle with one driving-and-steering wheel in the rear, as discussed in the previous section. Fig. 4 shows a conflict scenario of multiple vehicles represented by two forklifts. Let $\cup_{j=1}^m J_j$, $j = 1, 2, \ldots, m$, be the union of
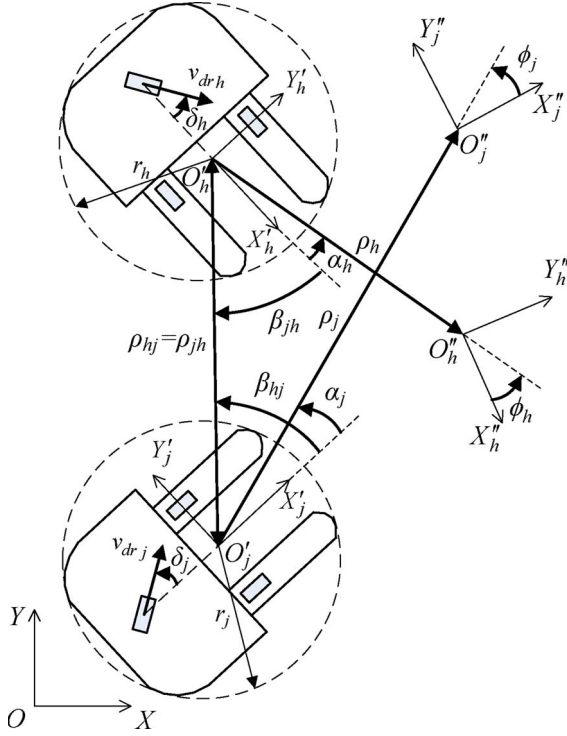
Fig. 4.   Conflict scenario of two forklifts.

circular vehicles in the workspace. The configuration and the radius of the jth vehicle is represented by (x_j, y_j, θ_j) and r_j, respectively. The navigation variables of a multivehicle system are denoted by $q = (q_1, \ldots, q_m)$, where $q_j = (\rho_j, \phi_j, \alpha_j)$ is the navigation variables of the jth vehicle. The control inputs for the jth vehicle are denoted by v_{dr_j} and δ_j.

In the case of multiple vehicles, the jth vehicle regards other vehicles as moving obstacles. From the perspective of the jth vehicle, $\cup_{h \neq j} H_h$ becomes the union of other vehicles in the workspace. A real-valued map $\Gamma_j : F \to R^+$ is defined as follows:

$$\Gamma_j = \prod_h \gamma_{hj} \qquad (38)$$

where $\gamma_{hj} = \rho_{hj}^2 - (r_j + r_h)^2$ and $\rho_{hj} = ((y_h - y_j)^2 + (x_h - x_j)^2)^{1/2}$. The zero value of Γ_j represents the boundaries of the collision-free areas of the jth vehicle to the union of the hth vehicle $\cup_{h \neq j} H_h$. Another real-valued map $\mathrm{B}_j : F \times \Theta \to R^+$ is defined as follows:

$$\mathrm{B}_j = \prod_h \beta_{hj}^2 \qquad (39)$$

where $\beta_{hj} = \mathrm{atan2}(y_h - y_j, x_h - x_j) - \theta_j$. The zero value of B_j denotes the jth vehicle's orientation, which is directed to

the union of the hth vehicles $\cup_{h \neq j} H_h$. Finally, a navigation function for multiple vehicles is defined as follows:

$$V_{\mathrm{mv}} = \sum_{j=1}^m V_{\mathrm{nh}_j} = \sum_{j=1}^m \frac{1}{2} \frac{z_j}{\left(z_j^\kappa + k_\gamma \Gamma_j + k_\beta \mathrm{B}_j\right)^{\frac{1}{\kappa}}} \qquad (40)$$

where $z_j = k_\rho \rho_j^2 + k_\phi \phi_j^2 + k_\alpha \alpha_j^2$.

The dynamics of variables γ_{hj} and β_{hj} are derived as follows:

$$\dot{\gamma}_{hj} = -2\rho_{hj}(v_{dr_j} \cos \beta_{hj} \cos \delta_j + v_{dr_h} \cos \beta_{jh} \cos \delta_h) \qquad (41)$$

$$\dot{\beta}_{hj} = (v_{dr_j}/\rho_{hj}) \sin \beta_{hj} \cos \delta_j + (v_{dr_j}/l) \sin \delta_j$$
$$+ (v_{dr_h}/\rho_{jh}) \sin \beta_{jh} \cos \delta_h + (v_{dr_j}/l) \sin \delta_h \qquad (42)$$

where $\rho_{hj} = \rho_{jh}$. The kinematics control law for multiple vehicles is stated below.

Proposition 3: Consider a multivehicle system consisting of m-vehicles, where each vehicle satisfies the dynamics of navigation variables (6)–(8). By implementing (34) and (35) for each vehicle, the origin of the closed-loop system is asymptotically stable.

Proof: Let the navigation function in (40) be a Lyapunov function candidate for a multivehicle system. By implementing (34) and (35) for each vehicle and by using (41) and (42), the time derivative of the Lyapunov function is derived as shown in (43) at the bottom of the page, where

$$\bar{\zeta}_j = \frac{z_j}{\kappa} \sum_h \left(\psi'_{\gamma_j} \frac{\rho_{hj}}{\gamma_{hj}} \cos \beta_{jh} - \psi'_{\beta_j} \left(\frac{\sin \beta_{jh}}{\beta_{hj} \rho_{jh}} + \frac{\tan \delta_h}{l_h} \right) \right)$$
$$\times v_{dr_h} \cos \delta_h. \qquad (44)$$

The derivative of a Lyapunov function of individual vehicles $\dot{V}_{\mathrm{nh}_j}$ in (43) has the same term as in (37), except for the variable $\bar{\zeta}_j$ at the third term of (43). At the origin, the value of $\bar{\zeta}_j$, as well as the values of $\bar{\rho}_j$, $\bar{\alpha}_j$, and $\bar{\xi}_j$, are zero since $z_j = 0$. By the same argument as stated in Proposition 2, the navigation variables of every vehicle are driven to the origin as $t \to \infty$; accordingly, $q_j(\infty) = (0, 0, 0)$. Finally, all trajectories from any initial conditions of the multivehicle system $q(0)$ converge to zero as $t \to \infty$. ∎

Upon the definition of a navigation function, the availability of a collision-free area is assumed. As stated in Definition 1, a navigation function maps the domain of a collision-free area to a real number. Thus, the existence of a collision-free area is required during the multiple-vehicle navigation. Updating the collision-free area during the multiple-vehicle navigation is under our investigation.

$$\dot{V}_{\mathrm{mv}} = \sum_{j=1}^m \dot{V}_{\mathrm{nh}_j} = \sum_{j=1}^m (\psi_{\gamma_j} + \psi_{\beta_j}) \left(\left(-k_{v_{dr}}(k_\rho \rho_j \cos \alpha_j - \bar{\rho}_j)^2 - k_{\alpha c} k_\alpha \alpha_j^2 (1 - \bar{\alpha}_j)^2 \right. \right.$$
$$\left. \left. + \bar{\alpha}_j \left(k_{v_{dr}}(k_\alpha \alpha_j + k_\phi \phi_j) \left(k_\rho \cos \alpha_j - (\bar{\rho}_j/\rho_j) \right) \sin \alpha_j - k_\alpha \alpha_j \bar{\xi}_j \right) \right) \cos \delta_j + \bar{\zeta}_j \right) \qquad (43)$$
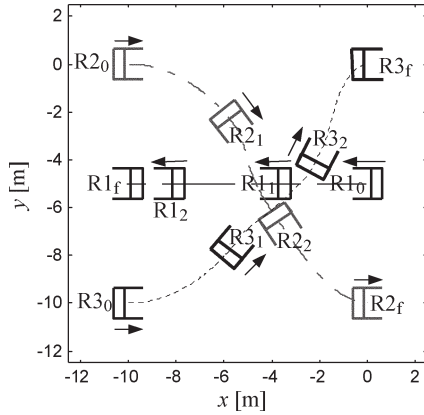
Fig. 5. Motions of three vehicles reaching their targets while avoiding moving vehicles (no static obstacles).

The proposed navigation scheme deals with either static obstacles or neighboring vehicles. If static obstacles exist, they are regarded as immobilized vehicles. In Proposition 3, the control inputs of the hth vehicle, which are v_{dr_h} and δ_h, are not included in the control law. However, the hth vehicle implements the same control law as the jth vehicle. Thus, their driving velocities v_{dr_h} approach zero as they reach their goal configurations. In (44), we can clearly see that $\overline{\zeta}_j, \forall j = 1, 2, \ldots, m$, converges to zero. In turn, the derivative of Lyapunov function (43) becomes the summation of the derivative of Lyapunov function (37) of all vehicles.

VI. SIMULATION AND EXPERIMENTAL RESULTS

A. Simulations

In this section, we verify the effectiveness of the proposed algorithm. The configuration of each vehicle is represented by (x, y, θ) (where the unit of x and y is meter and that of θ is radian) and the position of a static obstacle is represented by (x, y). The radius of each vehicle is set to 1 m.

In the first simulation, three vehicles Rj ($j = 1, 2, 3$) starting from R1$_0 = (0, -5, \pi)$, R2$_0 = (-10, 0, 0)$, and R3$_0 = (-10, -10, 0)$ will be driven by control law (34) and (35) to their targets at R1$_f = (-10, -5, \pi)$, R2$_f = (0, -10, 0)$, and R3$_f = (0, 0, 0)$, respectively. In this case, no static obstacles are assumed in the workspace. The used gains are $k_\rho = k_\alpha = k_\phi = 1$, $k_{v_{dr}} = 0.5$, $k_{\alpha c} = 1$, $k_\gamma = 0.3$, and $k_\beta = 35$. The tuning parameter is set at $\kappa = 60$. Fig. 5 shows the motions of the three vehicles. The intermediate positions (Rj_1 and Rj_2) in the middle of the paths are snapshots of the three vehicles at time 1 s and 3 s, respectively. Fig. 6 shows the control signals. In Fig. 6(b) and (c), it is shown that the vehicles R2 and R3 generate reverse motions (their driving velocities become negative) to allow R1 to reach its target. Then, the vehicles R2 and R3 reach their targets while avoiding collisions among them.

In the second simulation, a static obstacle of radius 1 m is placed at $(-5, -5)$, see Fig. 7. The initial-final configurations, the gains, and the parameters used in the second simulation are the same as before. Since the term $1/\beta_i$ appears in the variable $\overline{\alpha}$ in (25), the value of β_i is set to a positive (or negative) small value (in our simulation, 10^{-6} is used) when β_i becomes zero. In the initial configuration of R1, the value of α was
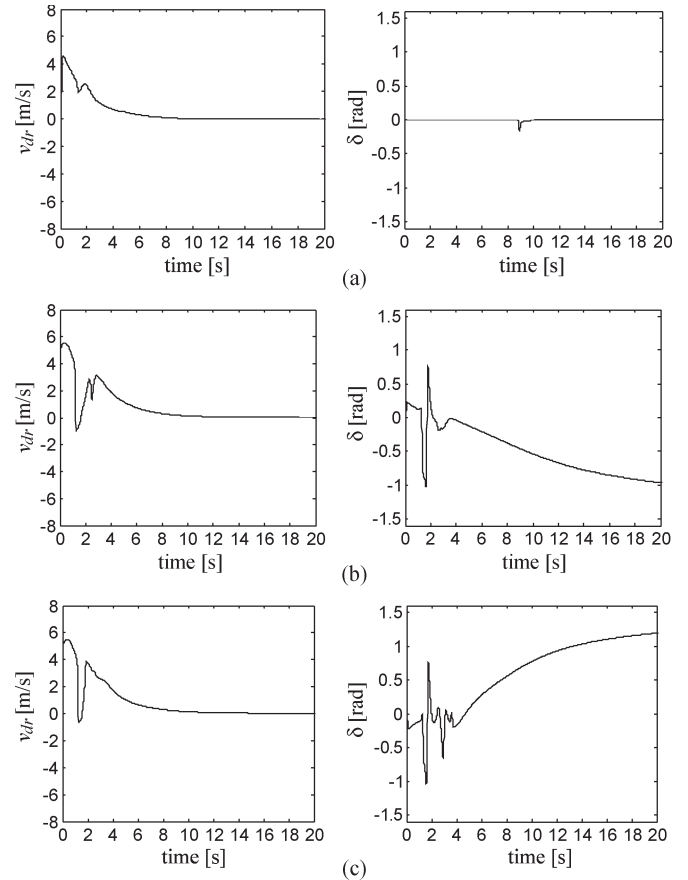
Fig. 6. Control input signals of the three vehicles reaching their targets while avoiding moving vehicles (no static obstacles). (a) Vehicle R1. (b) Vehicle R2. (c) Vehicle R3.
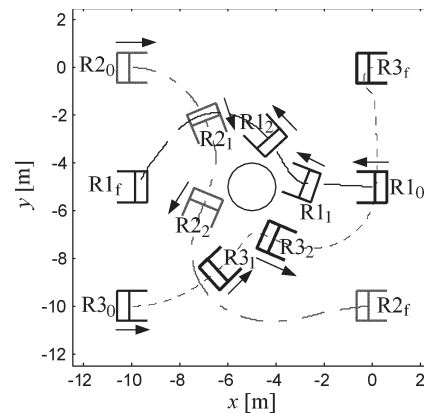
Fig. 7. Motions of three vehicles reaching their targets while avoiding moving vehicles and a static obstacle.

small. Therefore, $k_{\alpha c}\alpha(1 - \overline{\alpha})$ and $(k_\rho \cos \alpha - \overline{\rho}/\rho) \sin \alpha$ in (35) were small as well. The steering angle control signal δ is now determined by $\overline{\overline{\xi}}$. For a small positive β_i and $k_\rho \rho \cos \alpha - \overline{\rho} > 0$, the value of $\overline{\overline{\xi}}$ in (26) becomes positive. From (35), the steering angle control signal δ becomes positive, which provides a negative rotational velocity in (5) (turning in the counterclockwise direction). In response to the turning of R1 in the counterclockwise direction, the other vehicles R2 and R3 follow in the same direction. In Fig. 7, all the three vehicles reach their goal configurations while avoiding collisions among
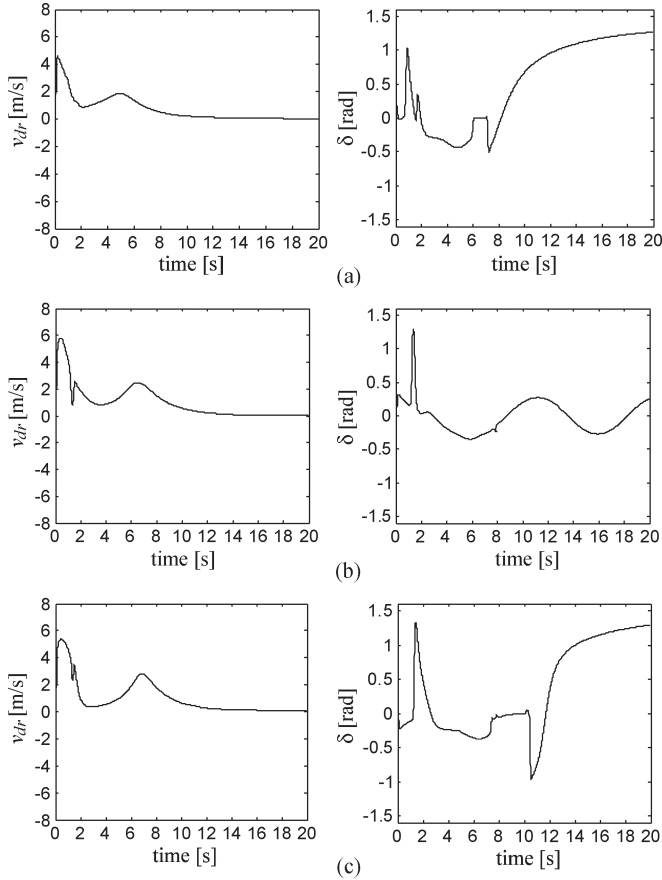
Fig. 8.   Control input signals of the three vehicles reaching their targets while avoiding moving vehicles and a static obstacle. (a) Vehicle R1. (b) Vehicle R2. (c) Vehicle R3.

them and with the static obstacle. The control input signals of the second simulation are given in Fig. 8. In Figs. 6 and 8, smooth control inputs signals are produced from the control laws of both simulations.

In the third simulation, two groups of vehicles (each group consists of four vehicles and the first and second groups of the vehicles are denoted by R1–R4 and R5–R8, respectively) moving in opposite directions along a corridor will be driven to their targets by using the proposed navigation method. The walls of the corridor are regarded as a series of point-obstacles ($r_i = 0$) along the two lines $y = 3$ and $y = -6$. The following configurations have been chosen: the initial configurations are $R1_0 = (-20, 0, 0)$, $R2_0 = (-14, 0, 0)$, $R3_0 = (-20, -3, 0)$, $R4_0 = (-14, -3, 0)$, $R5_0 = (4, 0, \pi)$, $R6_0 = (4, -3, \pi)$, $R7_0 = (10, 0, \pi)$, and $R8_0 = (10, -3, \pi)$; and the desired goal configurations are $R1_f = (4, 0, 0)$, $R2_f = (10, 0, 0)$, $R3_f = (4, -3, 0)$, $R4_f = (10, -3, 0)$, $R5_f = (-20, -3, \pi)$, $R6_f = (-14, -3, \pi)$, $R7_f = (-20, 0, \pi)$, and $R8_f = (-14, 0, \pi)$. The used gains are the same as in the previous simulations. The tuning parameter is set at $\kappa = 40$. As shown in Fig. 9, it is observed that all the vehicles reach their goal configurations while avoiding collision with the static obstacles (the walls) and among them.

B. Experimental Results

Fig. 10 shows the forklift used in experiment. The forklift has two AC motors to drive and steer the rear wheel, which are

controlled by a programmable logic controller (PLC). The cycle time of the digital proportional-integral-derivative controller for controlling the motors is 10 ms. The motion control algorithm programmed in C++ runs on an industrial PC (Pentium 1.4 GHz) with sampling time 100 ms. The PLC and the industrial PC communicate via RS232. The forklift is equipped with a laser-based localization sensor SICK NAV200 that provides a measurement of the forklift's position and orientation and with a laser range finder Hokuyo URG-04LX (range 4 m) that provides the measurement of the distance and the angle to obstacles. The target configuration is set to (0, 0, 0). The maximum value of the driving velocity is set to 10 cm/s. The obstacles are regarded as a series of point-obstacles (with no *a priori* knowledge on the positions of obstacles). The gains are set as follows: $k_\rho = k_\alpha = k_\phi = 1$, $k_{v_{dr}} = 1$, $k_{\alpha c} = 1.5$, $k_\gamma = 1$, and $k_\beta = 20$. The parameter is set at $\kappa = 70$.

In the first experiment, the initial configuration of the forklift is set to $(-6.32, 2.97, -0.73)$. Two static obstacles are placed at arbitrary positions. Fig. 11 shows the motion of the forklift in the X–Y coordinates and the control inputs v_{dr} and δ. A series of point-obstacles captured by the Hokuyo sensor is also shown in Fig. 11(a). The reaching of the forklift to its goal configuration at $(-0.067, 0.003, -0.017)$ is confirmed.

In the second experiment, the initial configuration of the forklift is $(-6.43, 2.84, -0.77)$. Two moving obstacles (persons) are assigned to pass through in front of the forklift while the forklift moves toward its goal configuration. Fig. 12 shows the motion of the forklift in the X–Y coordinates and the control inputs v_{dr} and δ. The discrete locations of moving persons are also indicated in Fig. 12(a). To avoid the moving obstacles, the navigation function-based control performs a real-time motion replanning based upon the positions of the obstacles measured by the Hokuyo sensor. The final configuration of the forklift is at $(-0.067, 0.003, -0.017)$.

VII. CONCLUSION

In this paper, a new navigation function for the case of nonholonomic systems has been proposed. The control law derived from the proposed navigation function guaranteed the asymptotic stability of the closed-loop system with collision avoidance properties. No chattering phenomenon of the closed-loop system was seen. The effectiveness of the navigation method was confirmed using the simulations of three and eight vehicles, and the experimental results that achieved the goal configuration while avoiding collisions among them in the presence of static and moving obstacles in the environment. The proposed algorithm was proven to be successful in driving the forklift from an arbitrary initial configuration to a goal configuration while avoiding collision with static and moving obstacles.

APPENDIX

A systematic method to determine the tuning parameter κ of the navigation function (16) is discussed. Let a new variable η be introduced as follows:

$$\eta \triangleq \eta_i \bar{\eta}_i^T \triangleq k_\gamma \prod_{i=1}^{n} \gamma_i + k_\beta \prod_{i=1}^{n} \beta_i^2 \tag{45}$$
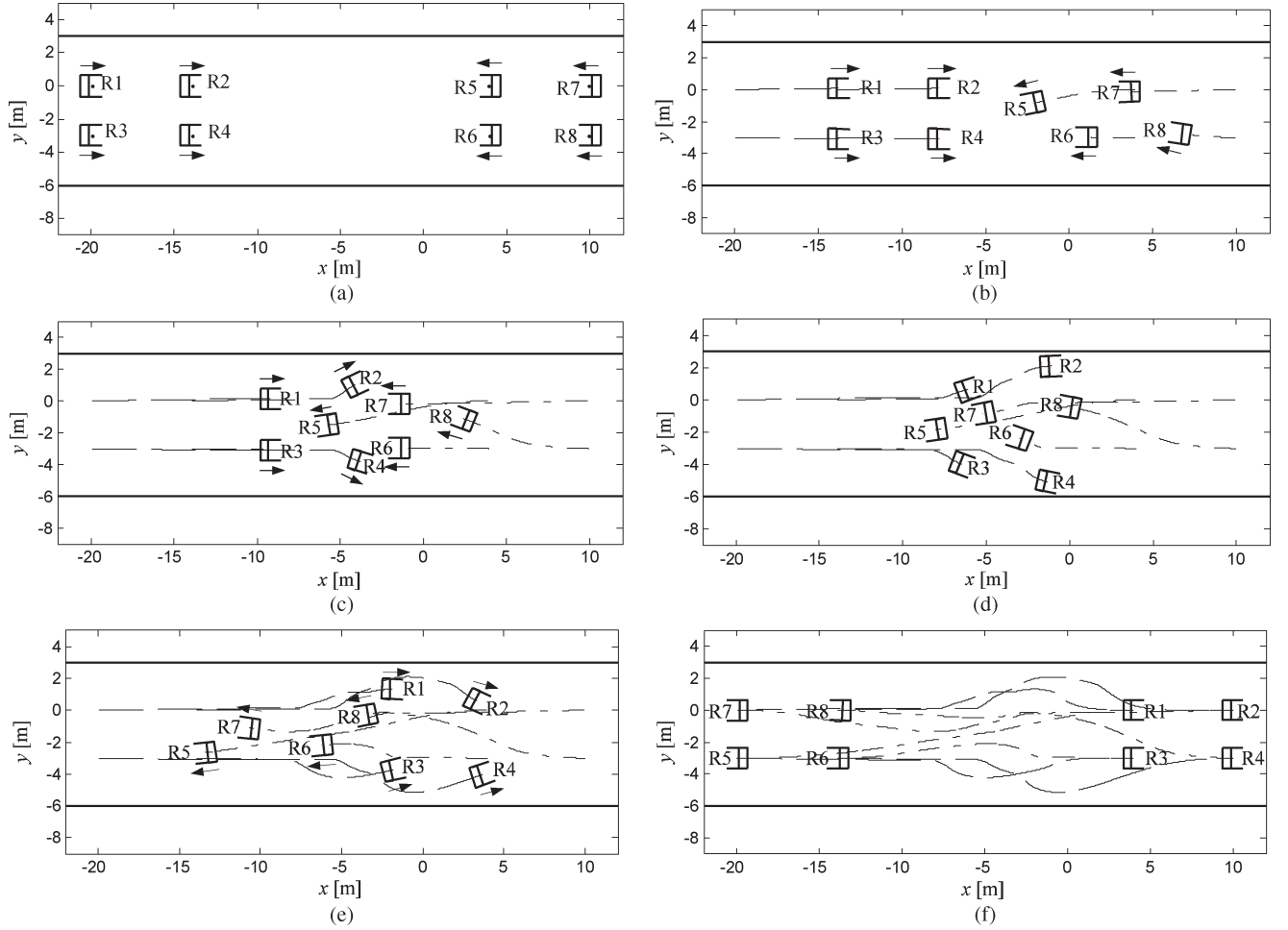
Fig. 9.   Motions of eight vehicles reaching their final configuration while avoiding collisions along a corridor. (a) $t = 0$ s. (b) $t = 10$ s. (c) $t = 20$ s. (d) $t = 30$ s. (e) $t = 50$ s. (f) $t = 200$ s.
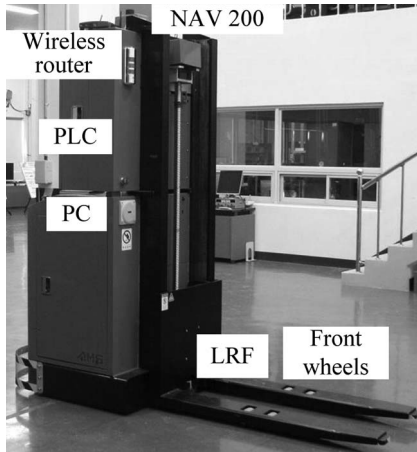
Fig. 10.   Forklift used in the experiment.

where

$$\eta_i \triangleq \left(\gamma_i, \beta_i^2 \right) \tag{46}$$

$$\overline{\eta}_i \triangleq \left(k_\gamma \prod_{j=0, j\neq i}^{n} \gamma_j, k_\beta \prod_{j=0, j\neq i}^{n} \beta_j^2 \right). \tag{47}$$

A function V'_{nh} is introduced as follows:

$$V'_{\mathrm{nh}} \triangleq z^\kappa / \eta. \tag{48}$$

Following the results in [12] and [32], all the critical points of V_{nh} (16) and V'_{nh} (48) are identical. Let F_1 be the collision-free area with no goal configuration.

Lemma 1: The goal configuration (x_d, y_d, θ_d) is a nondegenerate minimum of V_{nh}.

Proof: Taking the gradient of V_{nh} and noting $z(x_d, y_d, \theta_d) = 0$ and $\nabla z(x_d, y_d, \theta_d) = 0$, we have

$$\nabla V_{\mathrm{nh}}(x_d, y_d, \theta_d)$$
$$= \frac{1}{2(z^\kappa + \eta)^{2/\kappa}} \left((z^\kappa + \eta)^{1/\kappa} \nabla z - z \nabla (z^\kappa + \eta)^{1/\kappa} \right)$$
$$= 0. \tag{49}$$

Examining $\nabla^2 V_{\mathrm{nh}}$ at (x_d, y_d, θ_d), we obtain

$$\nabla^2 V_{\mathrm{nh}}(x_d, y_d, \theta_d)$$
$$= \frac{1}{2(z^\kappa + \eta)^{2/\kappa}} \left(2(z^\kappa + \eta)^{1/\kappa} I - z^2 \nabla (z^\kappa + \eta)^{1/\kappa} \right)$$
$$= \eta^{-1/\kappa} I. \tag{50}$$
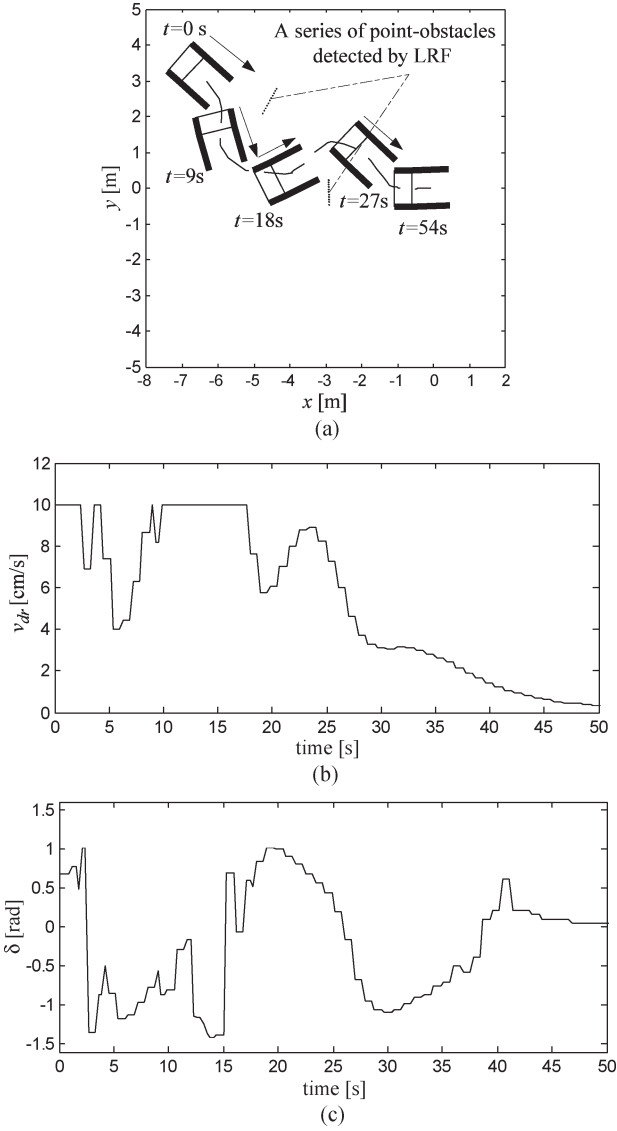
Fig. 11. Experimental results of reaching target while avoiding static obstacles. (a) Motion. (b) Driving velocity v_{dr}. (c) Steering angle δ.

This implies that (x_d, y_d, θ_d) is a nondegenerate minimum of V_{nh}. ∎

Lemma 2: For any $\varepsilon > 0$, there exists a positive integer $T(\varepsilon)$, such that if $\kappa \geq T(\varepsilon)$, then there are no critical points of V_{nh} in F_1.

Proof: At a critical point of V'_{nh}, we have

$$\kappa \eta \nabla z = z \nabla \eta. \tag{51}$$

Taking the magnitude of both sides of (51), we obtain

$$\kappa = \sqrt{z} \|\nabla \eta\| / (2\eta). \tag{52}$$

For $\|\eta_i\| \geq \varepsilon$, the upper bound of the right-hand side of (52) is given by

$$\sqrt{z} \|\nabla \eta\| / (2\eta) \leq (1/2) \sqrt{z} \sum_{i=0}^{n} \left(\|\bar{\eta}_i\| / \eta \right) \|\nabla \eta_i\|$$

$$< \frac{1}{2\varepsilon} \max_{W} \sqrt{z} \max_{W} \sum_{i=0}^{n} \|\nabla \eta_i\| \stackrel{\Delta}{=} T(\varepsilon). \tag{53}$$
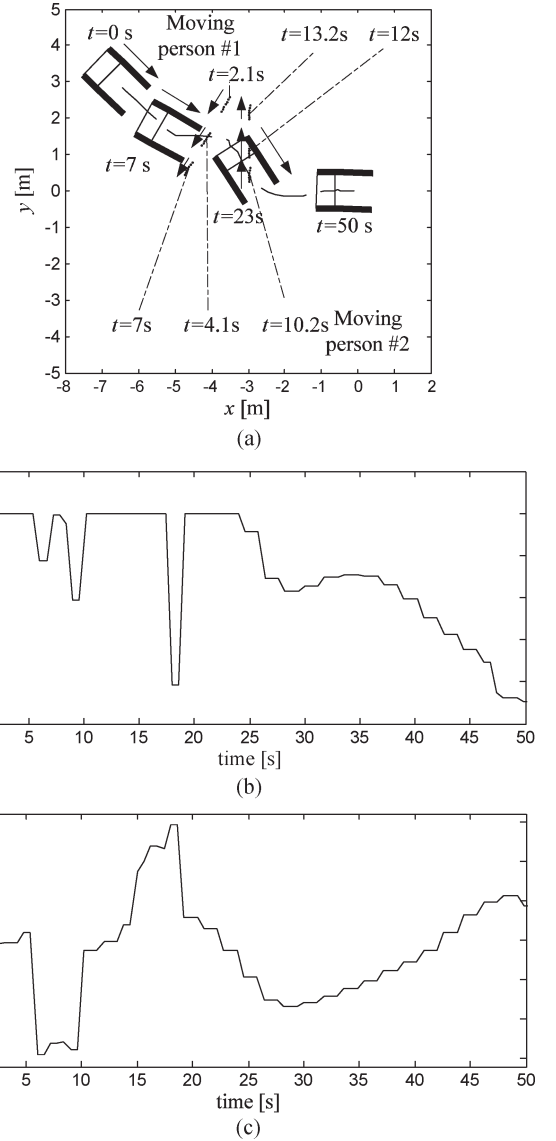
Fig. 12. Experimental results of reaching target while avoiding two moving persons. (a) Motion. (b) Driving velocity v_{dr}. (c) Steering angle δ.

If we choose

$$\kappa \geq T(\varepsilon) \tag{54}$$

then (51) does not hold, which implies that there are no critical points of V'_{nh}, as well as V_{nh}, in F_1. ∎

REFERENCES

[1] R. W. Brockett, "Asymptotic stability and feedback stabilization," in *Differential Geometric Control Theory*, R. W. Brockett, R. S. Millman, and H. J. Sussman, Eds. Boston, MA: Birkhäuser, 1983, pp. 181–191.

[2] R. M. Murray and S. S. Sastry, "Nonholonomic motion planning: Steering using sinusoids," *IEEE Trans. Autom. Control*, vol. 38, no. 5, pp. 700–716, May 1993.

[3] P. Souéres and J. P. Laumond, "Shortest paths synthesis for a car-like robot," *IEEE Trans. Autom. Control*, vol. 41, no. 5, pp. 672–688, May 1996.

[4] A. Widyotriatmo, B. Hong, and K.-S. Hong, "Predictive navigation of an autonomous vehicle with nonholonomic and minimum turning radius constraints," *J. Mech. Sci. Technol.*, vol. 23, no. 2, pp. 381–388, Feb. 2009.

[5] C. Samson, "Control of chained systems application to path following and time-varying point stabilization of mobile robots," *IEEE Trans. Autom. Control*, vol. 40, no. 1, pp. 64–77, Jan. 1995.

[6] A. Astolfi, "Discontinuous control of nonholonomic systems," *Syst. Control Lett.*, vol. 27, no. 1, pp. 37–45, Jan. 1996.

[7] T. A. Tamba, B. Hong, and K.-S. Hong, "A path following control of an unmanned autonomous forklift," *Int. J. Control Autom. Syst.*, vol. 7, no. 1, pp. 113–122, Feb. 2009.

[8] R. Olfati-Saber, A. Fax, and R. M. Murray, "Consensus and cooperation in networked multi-agent systems," *Proc. IEEE*, vol. 95, no. 1, pp. 215–233, Jan. 2007.

[9] W. Dong and J. A. Farrel, "Cooperative control of multiple nonholonomic mobile agents," *IEEE Trans. Autom. Control*, vol. 53, no. 6, pp. 1434–1448, Jul. 2008.

[10] M. Defoort, T. Floquet, A. Kökösy, and W. Perruquetti, "Sliding-mode formation control for cooperative autonomous mobile robots," *IEEE Trans. Ind. Electron.*, vol. 55, no. 11, pp. 3944–3953, Nov. 2008.

[11] J. Ghommam and F. Mnif, "Coordinated path-following control for a group of underactuated surface vessels," *IEEE Trans. Ind. Electron.*, vol. 56, no. 10, pp. 3951–3963, Oct. 2009.

[12] D. V. Dimarogonas, S. G. Loizou, K. J. Kyriakopoulos, and M. M. Zavlanos, "A feedback stabilization and collision avoidance scheme for multiple independent non-point agents," *Automatica*, vol. 42, no. 2, pp. 229–243, Feb. 2006.

[13] K.-S. Hong, T. A. Tamba, and J. B. Song, "Mobile robot architecture for reflexive avoidance of moving obstacles," *Adv. Robot.*, vol. 22, no. 13/14, pp. 1397–1420, Dec. 2008.

[14] A. A. Masoud, "Managing the dynamics of harmonic potential field-guided robot in a cluttered environment," *IEEE Trans. Ind. Electron.*, vol. 56, no. 2, pp. 488–496, Feb. 2009.

[15] Y. Hu, W. Zhao, and L. Wang, "Vision-based target tracking and collision avoidance for two autonomous robotic fish," *IEEE Trans. Ind. Electron.*, vol. 56, no. 5, pp. 1401–1410, May 2009.

[16] T. T. Q. Bui and K.-S. Hong, "Sonar-based obstacle avoidance using region partition scheme," *J. Mech. Sci. Technol.*, vol. 24, no. 1, pp. 365–372, Jan. 2010.

[17] J. C. Latombe, *Robot Motion Planning*. Norwell, MA: Kluwer, 1991.

[18] S. S. Ge and F. L. Lewis, Eds., *Autonomous Mobile Robots: Sensing, Control, Decision Making, and Applications*. Boca Raton, FL: CRC Press, 2006.

[19] J. Barraquand and J. C. Latombe, "Nonholonomic multibody mobile robots: Controllability and motion planning in the presence of obstacles," in *Proc. IEEE Int. Conf. Robot. Autom.*, Sacramento, CA, 1991, pp. 2328–2335.

[20] T. W. Manikas, K. Ashenayi, and R. L. Wainwright, "Genetic algorithms for autonomous robot navigation," *IEEE Instrum. Meas. Mag.*, vol. 10, no. 6, pp. 26–31, Dec. 2007.

[21] K. G. Chae and J. H. Park, "Trajectory optimization with GA and control for quadruped robots," *J. Mech. Sci. Technol.*, vol. 23, no. 1, pp. 114–123, Jan. 2009.

[22] R.-J. Wai and C.-M. Liu, "Design of dynamic Petri recurrent fuzzy neural network and its application to path-tracking control of nonholonomic mobile robot," *IEEE Trans. Ind. Electron.*, vol. 56, no. 7, pp. 2667–2683, Jul. 2009.

[23] S. Hong, J.-S. Choi, H.-W. Kim, M.-C. Won, S.-C. Shin, J.-S. Rhee, and H. Park, "A path tracking control algorithm for underwater mining vehicles," *J. Mech. Sci. Technol.*, vol. 23, no. 8, pp. 2030–2037, Aug. 2009.

[24] J.-B. Song and K.-S. Byun, "Steering control algorithm for efficient drive of a mobile robot with steerable omni-directional wheels," *J. Mech. Sci. Technol.*, vol. 23, no. 10, pp. 2747–2756, Oct. 2009.

[25] G. Oriolo, A. De Luca, and M. Vendittelli, "WMR control via dynamic feedback linearization: Design, implementation, and experimental validation," *IEEE Trans. Control Syst. Technol.*, vol. 10, no. 6, pp. 835–852, Nov. 2002.

[26] S. Kim and F. C. Park, "Fast robot motion generation using principal components: Framework and algorithms," *IEEE Trans. Ind. Electron.*, vol. 55, no. 6, pp. 2506–2516, Jun. 2008.

[27] J.-H. Lee and W.-S. Yoo, "An improved model-based predictive control of vehicle trajectory by using nonlinear function," *J. Mech. Sci. Technol.*, vol. 23, no. 4, pp. 918–922, Apr. 2009.

[28] S. S. Ge, J. Wang, T. H. Lee, and G. Y. Zhou, "Adaptive robust stabilization of dynamic nonholonomic chained systems," *J. Robot. Syst.*, vol. 18, no. 3, pp. 119–133, Mar. 2001.

[29] O. Khatib, "Real-time obstacle avoidance for manipulator and mobile robots," *Int. J. Robot. Res.*, vol. 5, no. 1, pp. 90–98, Mar. 1986.

[30] S. S. Ge and Y. J. Cui, "Dynamic motion planning for mobile robots using potential field method," *Auton. Robots*, vol. 13, no. 3, pp. 207–222, Nov. 2002.

[31] S. S. Ge and C.-H. Fua, "Queues and artificial potential trenches for multirobot formations," *IEEE Trans. Robot.*, vol. 21, no. 4, pp. 646–656, Aug. 2005.

[32] D. E. Koditschek and E. Rimon, "Robot navigation functions on manifolds with boundary," *Adv. Appl. Math.*, vol. 11, no. 4, pp. 412–442, Dec. 1990.

[33] E. Rimon and D. E. Koditschek, "Exact robot navigation using artificial potential functions," *IEEE Trans. Robot. Autom.*, vol. 8, no. 5, pp. 501–518, Oct. 1992.

[34] H. G. Tanner, S. G. Loizou, and K. J. Kyriakopoulos, "Nonholonomic navigation and control of cooperating mobile manipulator," *IEEE Trans. Robot. Autom.*, vol. 19, no. 1, pp. 53–64, Feb. 2003.

[35] S. G. Loizou and K. J. Kyriakopoulos, "Navigation of multiple kinematically constrained robots," *IEEE Trans. Robot.*, vol. 24, no. 1, pp. 221–231, Feb. 2008.

[36] H. G. Tanner and K. J. Kyriakopoulos, "Backstepping for nonsmooth systems," *Automatica*, vol. 39, no. 7, pp. 1259–1265, Jul. 2003.

[37] M. Aicardi, G. Casalino, A. Bicchi, and A. Balestrino, "Closed loop steering of unicycle-like vehicles via Lyapunov techniques," *IEEE Robot. Autom. Mag.*, vol. 2, no. 1, pp. 27–35, Mar. 1995.

[38] C. Prieur and A. Astolfi, "Robust stabilization of chained system via hybrid control," *IEEE Trans. Autom. Control*, vol. 48, no. 10, pp. 1768–1772, Oct. 2003.

[39] T. C. Lee and Z. P. Jiang, "Uniform asymptotic stability of nonlinear switched systems with an application to mobile robots," *IEEE Trans. Autom. Control*, vol. 53, no. 5, pp. 1235–1252, Jun. 2008.

[40] A. Widyotriatmo, K.-S. Hong, and L. H. Prayudhi, "Robust stabilization of a wheeled vehicle: Hybrid feedback control design and experimental validation," *J. Mech. Sci. Technol.*, vol. 24, no. 2, pp. 513–520, Feb. 2010.

Augie Widyotriatmo received the B.Eng. and M.Eng. degrees in engineering physics from the Bandung Institute of Technology, Bandung, Indonesia, in 2002 and 2006, respectively. He is currently working toward the Ph.D. degree with the School of Mechanical Engineering, Pusan National University, Busan, Korea.

His research interests include robotics, nonholonomic systems, nonlinear systems, robust control, visual serving, and multivehicle systems.

Keum-Shik Hong (M'87) received the B.S. degree in mechanical design and production engineering from the Seoul National University, Seoul, Korea, in 1979, the M.S. degree in mechanical engineering from the Columbia University, New York, in 1987, and both the M.S. degree in applied mathematics and Ph.D. degree in mechanical engineering from the University of Illinois at Urbana–Champaign (UIUC), Urbana, in 1991.

From 1982 to 1985, he was with Daewoo Heavy Industries, Incheon, Korea, where he worked on vibration, noise, and emission problems of vehicles and engines. From 1991 to 1992, he was a Postdoctoral Fellow at UIUC. Since 1993, he has been with the School of Mechanical Engineering, Pusan National University, Busan, Korea, where he is currently a Professor. His current research interests include nonlinear systems theory, adaptive control, distributed parameter system control, robotics, vehicle control, and innovative control applications to engineering problems.

Dr. Hong serves as the Editor-in-Chief of the *Journal of Mechanical Science and Technology* and as an Associate Editor in various IEEE and IFAC conferences editorial boards. He also served as an Associate Editor for the *Journal of Control, Automation, and Systems Engineering* and has been serving as an Associate Editor for *Automatica* (2000–2006) and as an Editor for the *International Journal of Control, Automation, and Systems* (2003–2005). His laboratory, Integrated Dynamics and Control Engineering Laboratory, was designated as a National Research Laboratory by the Ministry of Science and Technology of Korea in 2003. He received the Fumio Harashima Mechatronics Award in 2003 and the Korean Government Presidential Award in 2007. He is a member of ASME, ICASE, KSME, KSPE, KIEE, and KINPR.